Journal of Building Engineering 103 (2025) 112157

Contents lists available at ScienceDirect

Journal of Building Engineering

journal homepage: www.elsevier.com/locate/jobe

Effects of local heating of phase change floor (PCF) on thermal comfort and energy efficiency

Tianyu Wang [a], Haichao Wang [a,b,*], Zhiwen Luo [c]

[a] School of Infrastructure Engineering, Dalian University of Technology, Dalian, 116024, China
[b] Department of Mathematics and Systems Analysis, Aalto University, School of Science, P.O. BOX 11100, Espoo, Finland
[c] Welsh School of Architecture, Cardiff University, Cardiff, UK

ARTICLE INFO

Keywords:
Phase change floor (PCF)
Local heating
Heating power
Thermal comfort
Numerical simulation

ABSTRACT

To promote the application of phase change floors (PCFs) in buildings, the study designs various local heating methods based on modular PCFs. The accuracy of the simulation results is verified by comparing them with the experimental data. The effects of different heating powers, heating positions, and surface materials on thermal comfort, energy efficiency, and operating cost of PCFs are then investigated. The results show that as the heating power rises, the indoor thermal comfort duration time increases. The maximum floor surface temperature is reduced by approximately 14 °C by raising the heating power from 28.4 % to 86.4 %, which effectively alleviates the local overheating issue. However, there is an optimum value for the heating power. In this study, the average daily electricity consumption ($Q_{E,d}$) and cost (C_d) of the PCF are lowest when the heating power is 71.6 %. When changing the heating position, a uniform distribution of the heating zone is a more favorable method. Although its $Q_{E,d}$ and C_d values are slightly higher, it has better thermal comfort. Furthermore, marble PCF demonstrates superior performance compared to wood PCF. Despite the uniform distribution of heating zones, the average indoor temperature of the PCF heating room with a wood floor fails to reach 18 °C for a longer time. Additionally, the $Q_{E,d}$ and C_d values are high, exceeding 23 kWh/day and 9 ¥/day, respectively. Determining suitable local heating conditions can provide a reference for practical engineering design and further improve the heating performance of PCFs.

Nomenclature

Abbreviations			
PCMs	phase change materials	HR	heat release
PCT	phase change temperature	HST	heat storage time
PCF	phase change floor	HRT	heat release time
PCFR	phase change floor room	SHS	sensible heat storage
PMFR	phase change marble floor room	LHS	latent heat storage
PWFR	phase change wood floor room	THS	total heat storage
per	periphery	RMSE	root mean square deviation
cen	central	MAE	mean absolute error
uni	uniform	MAPE	mean absolute percentage error

(*continued on next page*)

* Corresponding author. School of Infrastructure Engineering, Dalian University of Technology, Dalian, 116024, China.
E-mail address: haichaowang@dlut.edu.cn (H. Wang).

https://doi.org/10.1016/j.jobe.2025.112157
Received 13 November 2024; Received in revised form 4 February 2025; Accepted 16 February 2025
Available online 17 February 2025

(*continued*)

Abbreviations			
HS	heat storage		
Symbols			
c	specific heat capacity, kJ/kg·°C	E	energy saving rate
h	latent heat, kJ/kg	H	enthalpy, kJ/kg
m	mass, kg	N, M	number
x	simulation value, °C	T	temperature, °C or K
y	experimental value, °C	ΔT	difference in temperature, °C
α	constant temperature coefficient	σ_b	black-body radiation constant, W/m^2·K^4
β	liquid fraction	C_d	average daily electricity cost, ¥/day
λ	thermal conductivity, W/m·°C	P_h	heating power, kW
σ	stability coefficient	P_{power}	percentage of heating power
ρ	density, kg/m^3	Q_E	electric consumption, kWh
ε	emissivity	T_f	fluid temperature, K
Δt	duration time, h	Q_{PFs}	heat storage capacity, kJ
C	electricity price, ¥/kWh	t^*	dimensionless time
f_t	increase factor of the thermal comfort duration time		
h_c	convection heat transfer coefficient, W/m^2·K		
T_w	unheated surface average temperature, K		
r	conversion factors between hours and days, h/day		
Subscript			
a	air	*out*	outdoor
d	day	*va*	valley
f	floor	*ref*	refer
i, j	number of stages	*com*	comfort
p	phase change material	*tcd*	thermal comfort duration
s	storage	*tsr*	temperature stable range
r	release	*end*	end heat storage moment
pe	peak	*initial*	initial heat storage moment
sur	surface		

1. Introduction

With energy and climate issues becoming increasingly prominent, cleaner and low-carbon production and living styles are receiving increasing attention. The global effort to conserve energy and reduce emissions is yielding results, as evidenced by the deceleration in primary energy demand growth in 2022 compared to the previous year [1] and the comparatively modest increase in carbon emissions in 2023 compared to 2022, showing a reduction of approximately 490 million tons [2]. However, environmental problems remain severe, with current energy consumption still dominated by fossil energy (about 79.7 % [3]) and CO_2 emissions reaching a record high (37.4 billion tons [2]). Of these, the building sector accounts for a large share of the energy consumed and carbon emissions generated, with nearly half of its energy used for heating buildings and generating more than 80 % of the direct CO_2 emissions in the building sector [4]. As the building sector expands and heating areas continue to grow, carbon reduction in building heating has significant potential and urgency.

The replacement of fossil fuels by renewable energy sources for heating has become a common strategy for reducing emissions in buildings and has achieved significant results. However, these non-polluting energy sources also suffer from a significant mismatch between heat supply and demand in their application. To address this problem, various types of energy storage technologies have been introduced and developed. Among them, latent heat storage is a prevalent technology employed in building envelopes with the objective of mitigating energy consumption and maintaining thermal comfort. This is achieved by utilizing the property of phase change materials (PCMs) that store a sizeable quantity of latent heat at a nearly constant temperature during the phase change. Examples of such applications include phase change walls [5] and phase change floors (PCFs) [6].

Among the many heating methods, radiant floor heating offers better thermal comfort. The PCF introduces PCMs to the common floor, which expands its thermal storage capacity and further improves indoor thermal comfort [7]. Current research on PCFs focuses on four aspects: materials, structures, operating conditions, and control strategies. In terms of materials, most of the PCMs in PCFs are paraffinic organic materials [8], and some scholars have used inorganic hydration salts, such as $CaCl_2{\cdot}6H_2O$ [9]. Thermophysical properties, such as phase change temperature (PCT), thermal conductivity, and latent heat, are the focus of materials research. The optimal selection of the PCT depends on the prevailing heating conditions. Sun et al. [10] showed that in the PCT range of 17–31 °C, the suitable PCT for heat storage is 30–31 °C, and the PCT for cold storage is 17–18 °C. Lin et al. [11] proposed that the appropriate PCT should differ in cities with varying climatic conditions. The appropriate PCT is also affected by the position of the PCM [12]. There is also an optimal value for the thermal conductivity of PCMs. The range of suitable thermal conductivity given by Zhou et al. is 0.4–0.6 W/(m·°C) [13]. The greater the thermal conductivity of the PCM, the faster the temperature rise in the room [14], but the greater the fluctuation, which is not conducive to indoor thermal comfort [15]. The latent heat of the PCM is an important factor in determining the thermal storage capacity of a material. Jin et al. [16] found that the heat flux at the floor surface became more stable as latent heat increased. Xu et al. [17] analyzed the PCFs under different latent heat conditions (90–150 kJ/kg) and pointed out that latent heat

should exceed 120 kJ/kg. In addition, numerous researchers have conducted extensive studies on composite PCMs to obtain suitable thermophysical properties. Fu et al. [18] used glycine as a temperature modifier to change the PCT of the inorganic hydrated salt PCM. Wang et al. [19] significantly enhanced the thermal conductivity of the PCM by adding expanded graphite. Meanwhile, the preparation of various new composite PCMs can also effectively solve the problems of PCMs, such as supercooling, phase separation, and leakage.

In terms of structure, PCF is mainly composed of the surface layer, PCM energy storage layer, heating layer, and thermal insulation layer. To enhance heat transfer, Faraj et al. [20] designed staggered spacers with metallic wires to elevate the thermal conductivity of the energy storage layer. Ansuini et al. [21] improved thermal transfer between the PCM and the pipe by installing a special steel substrate. In order to realize energy storage in winter and summer, Jin et al. [16] also designed a double-layer energy storage structure, i.e., PCMs with different PCTs were vertically stacked as cold and heat storage layers. This method effectively reduced heating and cooling energy consumption. Moreover, the positions of the upper and lower cold and heat storage layers could affect indoor thermal comfort and the economy [22]. The heating layers of PCFs are mostly electric heating films and hot water coils, while Zhou et al. [23] pointed out that the capillary mat has a better heating and thermal storage effect after comparing the PE coil with capillary mat. Furthermore, a suitable capillary mat position and a larger tube diameter both lead to an accelerated phase change in the PCM [10]. Underfloor ventilation is also a viable way to supply energy to the floor [24].

In terms of operating conditions, there are optimal values for the electrical heating power and water supply temperature for PCFs. When the PCF is electrically heated, Niu et al. [25] found that the higher the electrical heating power, the shorter the time required for thermal energy storage by the PCM, but too high a power can also result in the waste of heat. When the PCF is heated by hot water, Beak et al. [26] showed that too low a water supply temperature was not conducive to the melting of PCM, and too high a temperature would lead to overheating of the floor, with the appropriate water supply temperature being 40–41 °C. In contrast, an increase in water supply flow rate has a relatively small effect, although it promotes the indoor temperature rise and PCM heat exchange [27]. In terms of control strategies, the application of PCFs has been shown to reduce the number of start-ups and stops of heating devices [28]. Moreover, by rationally utilizing the peak and valley electricity pricing policy, the intermittent heating method designed by Li et al. [29] effectively reduces the operating costs of PCFs. To further improve the system economy, Barzin et al. [30] proposed an operating cost-based control strategy, which controls the room temperature according to the real-time electricity price. In addition, Cesari et al. [31] devised a control strategy based on weather prediction, which analyzes outdoor meteorological parameters and thus regulates the indoor temperature. The application of this method could effectively mitigate the problem of overheating. In addition to the above studies, other research has been carried out, such as the integration of PCFs with phase change ceilings [32] and the application of PCFs in different regions [33].

Through the above organization, PCF research has been conducted in various aspects. However, there are still some pressing issues that need to be addressed in the current study. Firstly, in previous studies, the PCFs were mostly fully heated, i.e., all the floors in the room needed to be heated when heating, the heating flexibility was poor, the heating power was large, and the electricity consumption and operating costs of the floors were still relatively high. Secondly, PCFs are often viewed as a multi-layer structure consisting of the heating device, PCM, surface layers, etc. [34]. Current research has mostly focused on improving and optimizing PCFs in the vertical direction, such as by using double-layer PCMs [16,22], while the improvement and optimization of PCFs in the horizontal direction have often been neglected. Finally, there is still a lack of more intuitive quantitative indicators for evaluating the property of the stable range of indoor temperatures in rooms with PCFs.

To solve the above problems, this paper adopts a local heating method for phase change floor rooms (PCFRs) in order to reduce the operating energy consumption and cost of the room by reducing the heating power, adjusting the heating position, and changing the surface material. The study improves and optimizes the PCF in the horizontal direction, modularizes the PCF, divides the PCF

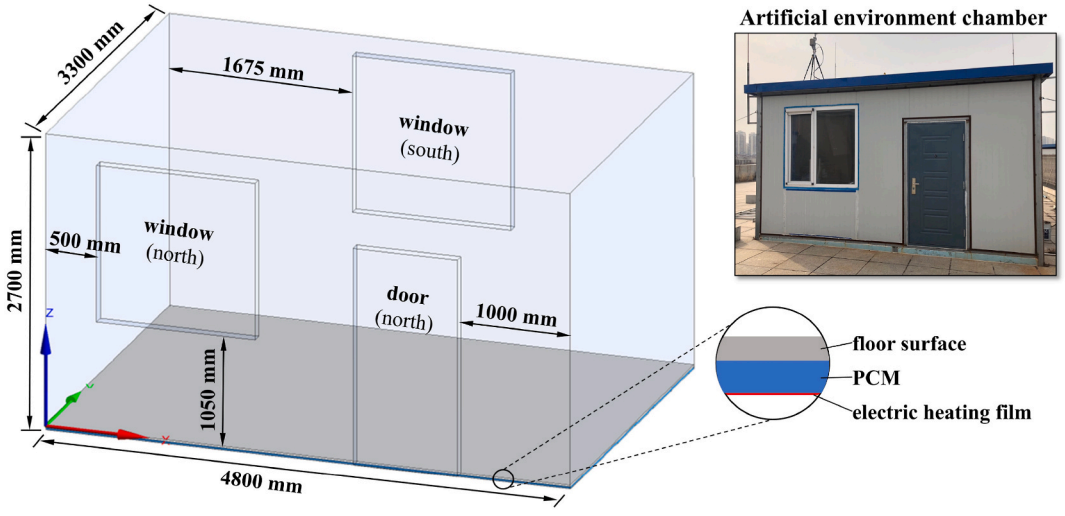

Fig. 1. Geometric model of the PCFR.

horizontally into many PCF modules that can be operated independently and heated flexibly. The heating power and heating position are changed by adjusting the opening and closing of the electric heating film in part of the PCF modules. In addition, the concept of room temperature stable range is proposed for the phenomenon of room temperature constancy existing in PCFRs, and the room temperature stable range is evaluated in terms of both relative stable temperature and duration time. Since numerous studies have analyzed the differences between common floor and PCF, this paper focuses on a comparative analysis of PCFRs. The study employs a combination of experimental and simulation methods to investigate the impact of local heating on thermal comfort and energy saving in PCFRs. The analysis considers various factors, including heating power, heating location, and surface material changes, and evaluates their influence across multiple indicators, such as average indoor temperature, heat storage and release time, stability coefficient, thermal comfort duration time increase factor, floor surface temperature, heat storage capacity, energy saving rate, and average daily electricity cost, etc. Exploring the local heating method of PCF and determining the appropriate heating power, heating position, and surface material provide guidance for practical engineering applications and help further reduce heating energy consumption and operating costs while maintaining indoor thermal comfort, thus promoting the application of PCF in buildings and advancing energy savings in buildings.

2. Methods

2.1. Simulation platform building

2.1.1. Geometric model

The room geometry was modeled based on an artificial environment chamber located in Dalian, China [35]. The floor arrangement and structural dimensions are shown in Fig. 1. The room dimensions are 4800 × 3300 × 2700 mm. PCF consists of the floor surface layer, PCM layer, and electric heating film. The thicknesses of the floor surfaces and PCM layers are 15 mm and 20 mm, respectively; the dimensions of both windows are 1450 × 1450 mm, and the door dimensions are 950 × 2000 mm. A comparative analysis of simulations under different conditions was carried out based on the room model. The study modeled a total of eight rooms (Table 1) under different conditions (heating power, heating location, and surface material). These include phase change marble floor rooms (PMFRs) with five different heating powers, denoted as 'PMFR-per1∼4 & PMFR-all'; two PMFRs with the same heating powers but different heating locations, denoted as 'PMFR-cen & PMFR-uni'; and a phase change wood floor room (PWFR) using wood as the surface material, denoted as 'PWFR-uni'.

P_{power} is the percentage of heating power, i.e. the ratio of room heating power to full heating power. For ease of presentation, the subsequent room heating power is expressed as P_{power}.

Fig. 2 shows the arrangement of heat sources for several local heating methods. The 'all' heating method means that all electric heating films are turned on. Since floor temperatures tend to be lower near the outdoors, a local heating method that prioritizes heating the perimeter is used. The 'periphery1∼4' heating methods indicate that the heating positions are the most peripheral one to four circles, respectively. The 'central' and 'uniform' heating methods indicate that the heating zones are arranged centrally and uniformly, respectively, with a guaranteed heating power of 71.6 %. Due to the different structural shapes of marble and wooden floors, the dimensions of the corresponding electric heating films are also different; their dimensions are 300 × 300 mm and 600 × 150 mm, respectively. To maintain the consistency of the heating power, the arrangement shown in Fig. 2 is used in the room with wooden floors.

2.1.2. Simulation settings

To simplify the simulation while ensuring accuracy, the study adopted the following assumptions: (1) The PCM is homogeneous without supercooling or phase separation; (2) The volume change during the PCM phase change is neglected; (3) The contact thermal resistance between materials is disregarded; (4) There is no heat exchange between the lower surface of the floor and the outside environment; (5) The temperature is the same at all points in the room at the initial moment; (6) The outdoor temperature is constant [14].

The energy equations for each material except PCM are [6]:

$$\rho c \frac{\partial T}{\partial t} = \lambda \nabla^2 T \tag{1}$$

Table 1
Room models for 8 different operating conditions.

Room	PMFR-per1	PMFR-per2	PMFR-per3	PMFR-per4
Add PCM	yes	yes	yes	yes
Heating method (P_{power})	periphery1 (28.4 %)	periphery2 (52.3 %)	periphery3 (71.6 %)	periphery4 (86.4 %)
Surface material	marble	marble	marble	marble
Room	PMFR-all	PMFR-cen	PMFR-uni	PWFR-uni
Add PCM	yes	yes	yes	yes
Heating method (P_{power})	all (100 %)	central (71.6 %)	uniform (71.6 %)	uniform (71.6 %)
Surface material	marble	marble	marble	wood

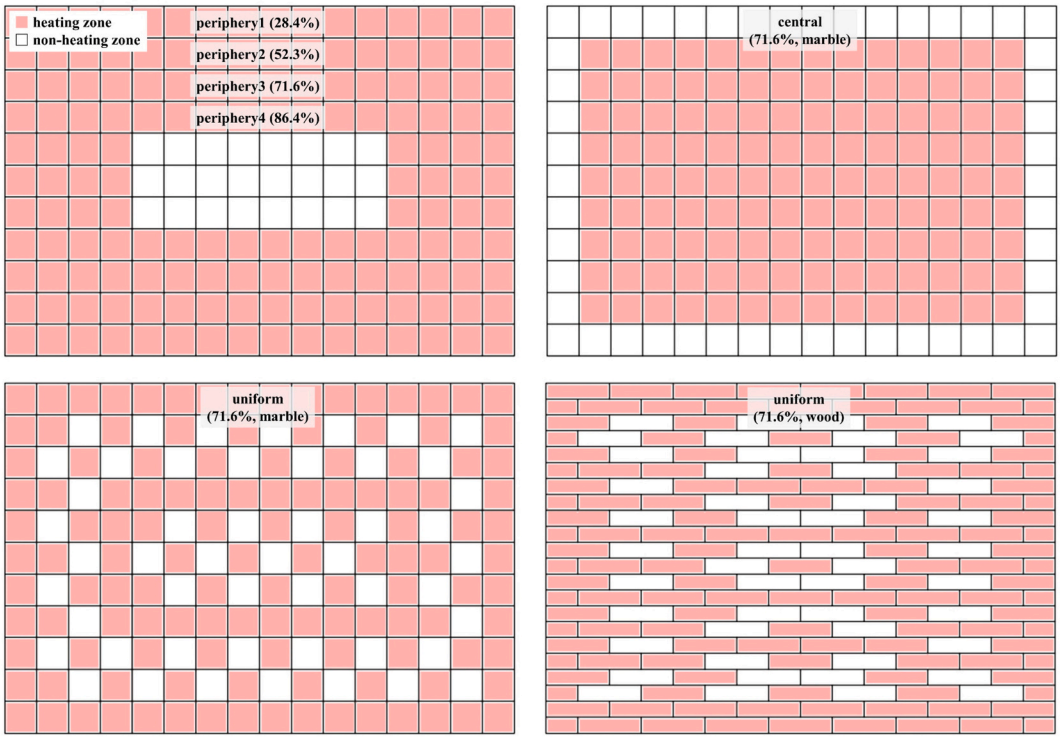

Fig. 2. Local heating method.

Where ρ, c, T, λ are density, kg/m^3, specific heat, kJ/kg·°C, temperature, °C, and thermal conductivity, W/m·°C, respectively.

The governing equation for the phase change region is [6]:

$$\rho_p \frac{\partial H}{\partial t} = \lambda_p \nabla^2 T \tag{2}$$

Where the subscript p refers to the PCM and H consists of the sensible enthalpy h_s and latent heat h:

$$H = h_s + \beta h \tag{3}$$

$$h_s = h_{ref} + \int_{T_{ref}}^{T} c_p dT \tag{4}$$

$$\beta = \begin{cases} 0, T < T_s \\ \dfrac{T - T_s}{T_l - T_s}, T_s < T < T_l \\ 1, T < T_l \end{cases} \tag{5}$$

where h_{ref} is the reference enthalpy, kJ/kg; T_{ref} is the reference temperature, °C; β is the liquid fraction; T_s and T_l are the temperatures at the beginning and end of the PCM solidification, °C, respectively.

Initial and boundary conditions [14,15]:

Initial moment:

$$T_{(x,y,z,t=0)} = T_{initial} \tag{6}$$

PCF perimeter and bottom surfaces:

$$\frac{\partial T}{\partial x} = \frac{\partial T}{\partial y} = \frac{\partial T}{\partial z} = 0 \tag{7}$$

The PCM surface inside the PCF is the coupled boundary with continuous temperature and heat flux:

$$T_{(x,y,z,t)}|_1 = T_{(x,y,z,t)}|_2 \tag{8}$$

$$-\lambda \frac{\partial T}{\partial n}|_1 = h_c (T - T_f)|_2 \tag{9}$$

PCF upper surface:

$$-\lambda \frac{\partial T}{\partial z} = h_c (T - T_a) + \varepsilon \sigma_b (T^4 - T_w^4) \tag{10}$$

Exterior wall surfaces of the room:

$$T = T_{out} \tag{11}$$

Where h_c is the convection heat transfer coefficient, W/m^2·K; ε is the emissivity; σ_b is the black-body radiation constant, W/m^2·K^4; T_f, T_a, T_{out} and T_w are the fluid, indoor air, outdoor and unheated surface average temperature, K, respectively.

Transient simulations were conducted using ANSYS Fluent simulation software. The Surface to Surface (S2S) radiation model [14] and melting/solidification model were adopted. The specific thermophysical parameters of the floor surface material and PCM are listed in Table 2. Parameters for other materials, such as walls, can be found in the literature [35]. The PCT of PCM is 28~30 °C, the latent heat is 150 kJ/kg, and the amount of PCM is approximately 256.61 kg. The study simulated the heat storage (HS) and heat release (HR) processes in each room. The electric heating film power is 220 W/m^2, the total heating area is 15.84 m^2, and the heating power is approximately 3.48 kW at full heating. The outdoor temperature was set to −9 °C [36]. At the initial moment, the indoor temperature was set to 18 °C, and heating began. Heating stopped when the indoor temperature reached 24 °C, marking the end of the HS process. The HR process was then carried out until the room temperature was reduced to 18 °C.

2.2. Model validation and independence test

A small box experimental platform (Fig. 3(a)) was set up to perform accurate checks of the simulation results. The platform includes a phase change marble floor box and a phase change wood floor box. Both boxes are surrounded by a 20 mm thick wooden shell, with 30 mm thick insulation panels attached to the shell and the PCF module at the bottom of the box. The PCF module structure is similar to that of the PCF in Fig. 1 and consists, from top to bottom, of surface material (marble/wood), PCM (paraffin), electric heating film, and insulation board. The dimensions of the marble and wood PCF modules are 150 × 150 mm and 450 × 150 mm, respectively. The thicknesses of the surface material and PCM are 15 mm and 30 mm, respectively. The electric heating film is equipped with an interface whereby the modules can be connected to each other for local heating. A temperature sensor with an accuracy of ±0.3 °C and a working range of −40 to 80 °C was used [39]. The variation in air temperature at 200 mm from the floor surface center in the vertical direction with time was monitored for the following four heating operating cases shown in Fig. 3(b). Case 1: Marble floor full power heating; Case 2: Marble floor local heating by X-crossing of five PCF modules; Case 3: Wood floor full power heating; Case 4: Wood floor local heating by two PCF modules on both sides. Meanwhile, the study established a box geometry model with the same dimensions as the experimental box. Simulations of HS and HR processes of the box with the same four cases as the experiments were carried out, and the temperature data at the same measurement point locations were recorded. The box simulation settings are essentially the same as the room simulation settings. The same simulation assumptions were used, and the same setup was performed in ANSYS Fluent software. The initial temperature of the box was set at 20 °C according to the actual conditions of the experiment.

The temperature data were experimentally monitored for four cases during the HS and HR processes. In order to minimize the experimental error, the study conducted six HS and HR processes for each of the heating conditions mentioned above (Case1/Case2/Case3/Case4) and took the average value as the experimental data for each case. As illustrated in Fig. 4, the simulation data exhibit a similar trend to the experimental data observed during the HS and HR processes. A discrepancy exists between the simulated and experimental values. This is due to the fact that the simulation process assumes a constant temperature for the outer wall of the box, ignores changes in the external temperature, and sets the initial temperature for all areas of the box at the same value. The maximum temperature deviation between the two values does not exceed 0.6 °C, and the error does not exceed 2.7 %. In addition, the root mean square deviation (RMSE), mean absolute error (MAE), and mean absolute percentage error (MAPE) were calculated according to Eq. (12)–(14) [40]. The results show that the maximum RMSE, MAE, and MAPE are only 0.3 °C, 0.23 °C, and 0.97 % for the four cases, respectively. As evidenced by the comparison of experimental and simulation results, the utility of the simulation approach for investigating the PCF is substantiated.

$$RMSE = \sqrt{\sum_{i=1}^{N} \frac{(x_i - y_i)^2}{N}} \tag{12}$$

Table 2
Thermophysical parameters of materials.

Materials	marble [37]	wood	PCM [38]
λ (W/m·°C)	3.5	0.173	0.21
ρ (kg/m^3)	2800	700	810
c (kJ/kg·°C)	1	2.31	2.14

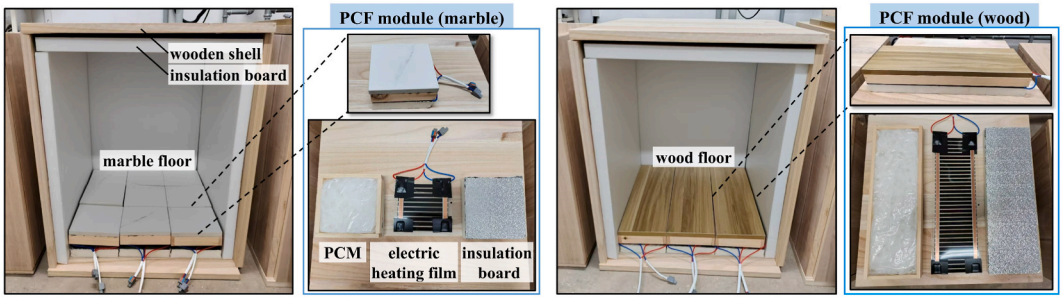

Fig. 3. The experimental platform and four heating cases for phase change marble and wood floors.

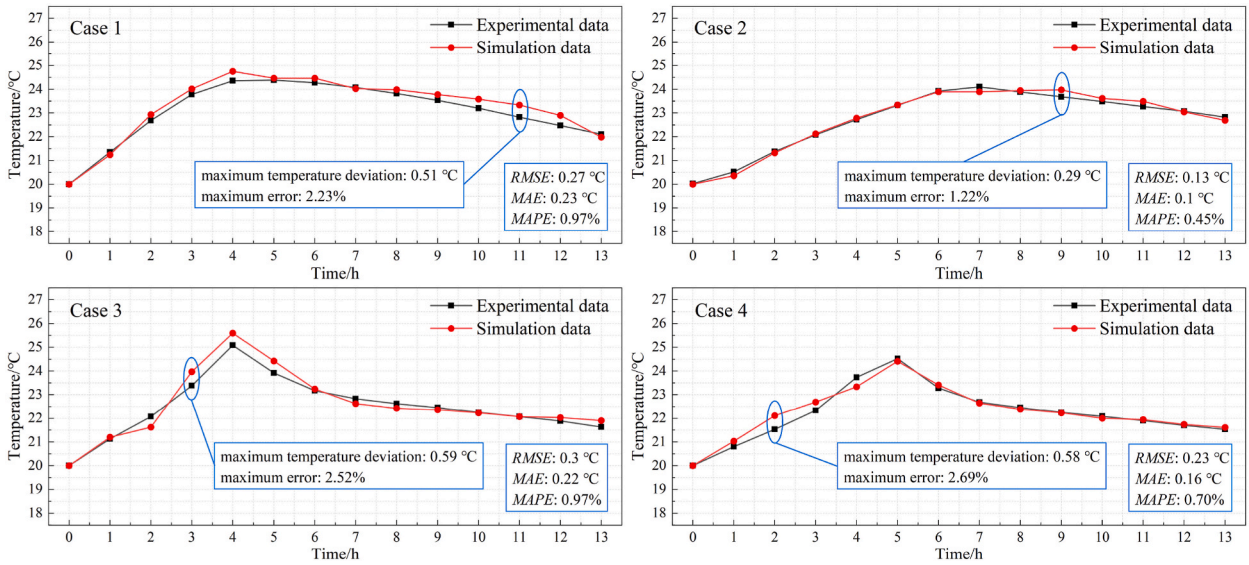

Fig. 4. Comparison of experimental and simulation data of box temperature measurement point.

$$MAE = \sum_{i=1}^{N} \frac{|x_i - y_i|}{N} \tag{13}$$

$$MAPE = \frac{1}{N} \sum_{i=1}^{N} \left| \frac{x_i - y_i}{y_i} \right| \times 100\% \tag{14}$$

where N is the number; x_i and y_i represent the simulated and experimental values at moment i, respectively.

In addition, mesh number and time step independence tests have been performed. Meshing was done using the Automatic method, and the grid was refined at doors, windows, floors, etc. The number of mesh comparisons ranged from 0.89 to 3.33 million. From Fig. 5

(a), the average indoor temperature changes as the number of meshes increases. When the number of meshes exceeds 1.6 million, the average indoor temperature changes are relatively small. In addition, time steps of 1–20 s were selected for comparison. From Fig. 5(b), the size of the time step has less effect on the average indoor temperature. When the time step is less than 10 s, the temperature basically does not change with the time step. Therefore, in order to save as much computational time as possible while ensuring the accuracy of the simulation results, the number of meshes was finally selected to be 1.6 million, and the time step was 10 s.

2.3. Performance evaluation indicators

The study not only analyzed the average indoor temperature, the floor surface temperature ($T_{f,sur}$), the PCM liquid fraction, the heat storage time (HST), and the heat release time (HRT), but also employed a series of evaluation indicators, including:

(1) Stability coefficient (σ) [41]

The stability coefficient can be used to evaluate the dispersion of the indoor temperature with respect to a defined thermal comfort temperature; the larger the σ value, the closer the indoor temperature is to that defined temperature.

$$\sigma = 1 - \frac{\sqrt{\sum_{i=1}^{N}(T_i - T_{com})^2/N}}{\sum_{i=1}^{N} T_i/N} \tag{15}$$

Where T_i is the average indoor temperature at moment i, °C; T_{com} is the defined thermal comfort temperature, taken as 24 °C.

(2) The increase factor of the thermal comfort duration time (f_t) [42]

The f_t is a thermal comfort evaluation parameter based on time scale. It represents the ratio of the time that the PCFR and reference room1 can maintain the indoor thermal comfort temperature (18–24 °C [43]) after the heating is stopped. PMFR-per1 with the shortest $\Delta t_{tcd,r}$ was selected as reference room1.

$$f_t = \Delta t_{tcd,r} / \Delta t_{ref,tcd,r} \tag{16}$$

Where $\Delta t_{tcd,r}$ and $\Delta t_{ref,tcd,r}$ are the time for which the PCFR and the reference room can maintain indoor thermal comfort after the heating is stopped, respectively, h.

(3) Relative stable temperature (T_{tsr}) and duration time (Δt_{tsr}) in room temperature stable range

Based on the thermostatic HS and HR properties of PCMs, there will be a room temperature stable range for PCFR, in which the indoor temperature is essentially constant or changes very little. Since the drastic degree of indoor temperature change directly affects the indoor thermal comfort, the study introduces the relative stable temperature T_{tsr} and duration time Δt_{tsr} to evaluate the thermostatic characteristics of the room temperature stable range. T_{tsr} is the average value of the temperature at all moments that satisfy the condition of constant temperature (Eqs. (18) and (19)) during HS/HR process. Δt_{tsr} is the duration time for which the constant temperature can be maintained. The higher the Δt_{tsr} value, the longer the constant temperature, the better the indoor thermal comfort.

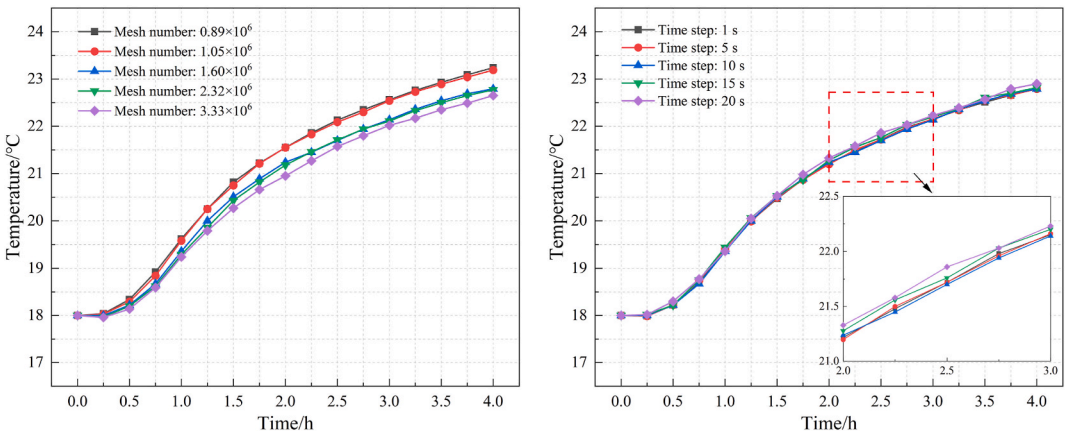

Fig. 5. Independence test for the mesh number and time step.

$$T_{tsr} = \frac{1}{M}\sum_{j=1}^{M} T_{tsr,j} \tag{17}$$

$$\left|T_{tsr,j+1} - T_{tsr,j}\right| \le \alpha(T_{end} - T_{initial}) \tag{18}$$

$$T_{inital} < T_{tsr,j} < T_{end} \tag{19}$$

where M is the number of moments that satisfy the constant temperature condition; $T_{tsr,j}$ and $T_{tsr,j+1}$ are the temperatures, °C, at the j and j+1 moments of satisfying the constant temperature condition, with a time interval of 0.5 h; α is the constant temperature coefficient, which is taken as 5 % in this paper; T_{end} and $T_{initial}$ are the indoor temperatures at the end and the beginning of thermal storage set by the study, which are 24 °C and 18 °C, respectively. That is, the study considers the range in which the temperature does not change by more than 0.01 °C/min as the temperature stable range.

(4) Heat storage capacity (Q_{PFs}) [44]

The total heat stored (THS) in the PCM of the PCF is mainly latent heat storage (LHS) and includes a certain amount of sensible heat storage (SHS), which can be expressed as:

$$Q_{PFs} = c_p m_p \Delta T_p + m_p h \tag{20}$$

where c_p, m_p, ΔT_p, and h are PCM specific heat, kJ/kg·°C, mass, kg/m^3, temperature change during HS, °C, and latent heat, kJ/kg, respectively.

(5) Energy saving rate (E) [33].

The energy saving rate is the ratio of the energy saved in the PCFR to reference room2, the larger the E value, the better the energy savings. In order to investigate the energy savings of each PCFR compared to the conventional PCFR, PMFR-all was selected as reference room2.

$$E = \frac{Q_E - Q_{ref,E}}{Q_{ref,E}} \tag{21}$$

where $Q_{ref,E}$ and Q_E are the electricity consumption of the reference room and the PCFR, kWh, respectively. Based on the average daily electricity cost [6], the average daily electricity consumption ($Q_{E,d}$) is used, which can be calculated according to the following equation:

$$Q_{E,d} = \frac{rP_h\Delta t_s}{\Delta t_s + \Delta t_r} \tag{22}$$

where r is the conversion factor between hours and days and is 24 h/day; P_h is the heating power of the electric heating film, kW; Δt_s and Δt_r are the turn-on and turn-off duration time of the electric heating film in a HS and HR cycle, respectively, h.

(6) Average daily electricity cost (C_d) [6]

The average daily electricity cost is the daily operating cost of the floor considering the difference in peak and valley electricity prices.

$$C_d = \frac{rP_h\left(C_{pe}\Delta t_{s,pe} + C_{va}\Delta t_{s,va}\right)}{\Delta t_s + \Delta t_r} \tag{23}$$

Where C_{pe} and C_{va} are the electricity price during peak and valley period, respectively, ¥/kWh; $\Delta t_{s,pe}$ and $\Delta t_{s,va}$ are the operating duration time of the electric heating film during peak and valley period, respectively, h.

3. Results and discussion

The rooms were divided into two groups for comparative analysis. (1) The PCFRs with different heating powers (PMFR-per1∼4 & PMFR-all); (2) The PCFRs with different heating positions and surface materials (PMFR-per3, PMFR-cen, PMFR-uni, PWFR-uni). The indoor thermal comfort was explored by analyzing the average indoor temperature, HST and HRT, stability coefficient (σ), thermal comfort duration time increase factor (f_t), relative stable temperature (T_{tsr}) and duration time (Δt_{tsr}) in the temperature stable range, as well as floor surface temperatures. Meanwhile, the PCM liquid fraction was also analyzed. The room energy efficiency was evaluated using the heat storage capacity (Q_{PFs}), energy savings rate (E), average daily electricity consumption ($Q_{E,d}$) and costs (C_d).

3.1. Analysis of the influence of different heating power

3.1.1. Thermal comfort analysis

Fig. 6 shows the variation in average indoor temperature with time during the HS and HR processes. When the heating power is very small, especially in PMFR-per1, the indoor temperature initially declines due to the low external temperature, then increases. When the heating power is greater than 52.3 %, this phenomenon essentially disappears, and the indoor temperature continues to increase. The temperature does not drop immediately after heating is stopped, and it is warmed up again for a period, during which the maximum temperature of PMFR-per2∼4 and PMFR-all exceeds 24 °C. The time consumed to raise the average indoor temperature from 18 °C to 24 °C is called the HST, and the time consumed to lower the temperature to 18 °C is called the HRT. During HS, the PCM temperature rises as it undergoes a period of SHS before and after melting. While PCM stores latent heat, its temperature remains essentially unchanged. This causes the indoor temperature change in PCFRs (PMFR-per2∼3&all) to show a trend of a steep rise followed by a slow climb and finally a steep rise again. Similarly, during HR, the PCM needs a period of time to first cool down to the PCT, then release the stored latent heat, and finally release the sensible heat again. Thus, there is a period of slowly decreasing indoor temperature in PCFRs. As the heating power of the room rises, the HST gradually decreases, while the HRT increases. This is mainly because the room temperature is affected by the heating power when storing heat: the more heating power, the faster the temperature rises. During the HR process, room heating mainly depends on the amount of heat stored in PCM. The HSTs of PMFR-per1∼4 and PMFR-all were 36.18 h, 9.91 h, 7.57 h, 6.63 h, and 5.97 h, respectively; the HRTs were 5.95 h, 10.07 h, 15.43 h, 17.39 h, and 18.68 h, respectively.

Table 3 summarizes the values of σ, f_t, and T_{tsr} for each room. Both the σ and f_t values grow progressively as the heating power increases. This means that the average indoor temperature during HS and HR processes is getting closer to the defined thermal comfort temperature of 24 °C as the room is heated with higher power, and that the temperature can be maintained between 18 and 24 °C for a longer duration during HR. PMFR-per1 is used as reference room1, and when the heating power exceeds 71.6 %, the f_t value reaches 2.34, and the HR thermal comfort time increases by more than a factor of 1. In addition, there is a relatively stable temperature range for the average indoor temperature when the PCFR is storing and releasing heat (Fig. 6). Due to the extremely long HST of PMFR-per1, the temperature always changes slowly throughout the HS process. Disregarding the special case of PMFR-per1, the T_{tsr} values of PMFR-per2∼4 and PMFR-all continue to increase with the increase in heating power. The T_{tsr} value is not less than 18.5 °C and reaches up to 23.2 °C. There are also differences in the relative stable temperatures during HS and HR in the same room. The higher the heating power, the more significant this difference becomes, with $T_{tsr,s}$ being higher than $T_{tsr,r}$ by about 1.2 °C in PMFR-all.

Fig. 7 shows the duration time of thermal comfort and stable temperature states in the HS/HR process, and the proportion of Δt_{tcd} occupied by Δt_{tsr}. In HS, thermal comfort duration time ($\Delta t_{tcd,s}$) and stable temperature range duration time ($\Delta t_{tsr,s}$) are negatively correlated with the variation of heating power. In HR, thermal comfort duration time ($\Delta t_{tcd,r}$) and stable temperature range duration time ($\Delta t_{tsr,r}$) are positively correlated with the heating power. Meanwhile, Δt_{tcd} and Δt_{tsr} are generally larger in HR than in HS, and this difference becomes more obvious with the increase of heating power. The differences ($\Delta t_{tcd,s}$ and $\Delta t_{tcd,r}$, $\Delta t_{tsr,s}$ and $\Delta t_{tsr,r}$) are 11.47 h and 12.5 h, respectively, when heated with full heating power. When the heating power is 52.3 %, both differences do not exceed 1 h. In addition, the percentage of the stable temperature range in the thermal comfort period is also influenced by heating power. With higher heating power, the percentage during HS is smaller, but the percentage during HR increases instead.

The temperature distribution of the floor surface at the end of the HS is illustrated in Fig. 8. Since the local heating positions of PMFR-per1∼4 are set around the room's perimeter, the distribution of $T_{f,sur}$ shows a trend of low in the middle and high around the perimeter. That is, a local overheating problem occurs at the heating positions. Additionally, along with the reduction in heating

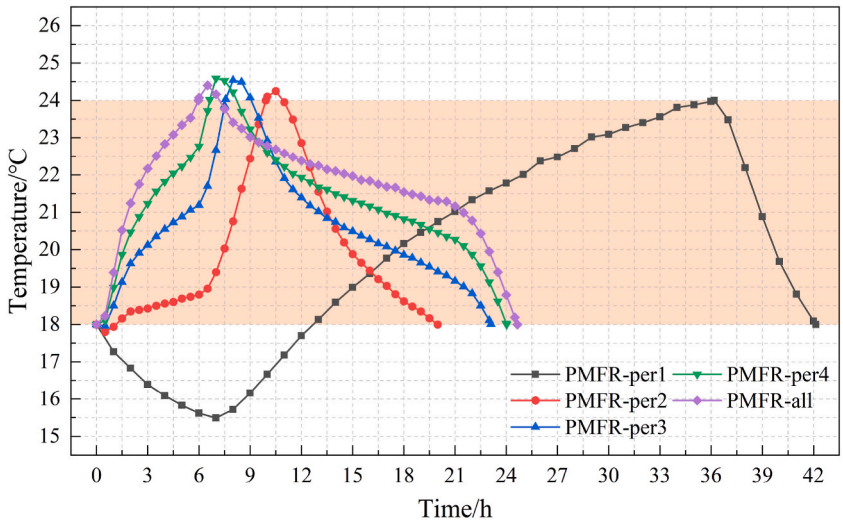

Fig. 6. Variation of average indoor temperature with time for different heating powers.

Table 3
Stability coefficient, thermal comfort duration time increase factor, relative stable temperature for each room.

Evaluation parameter	PMFR -per1	PMFR -per2	PMFR -per3	PMFR -per4	PMFR -all	PMFR -cen	PMFR -uni	PWFR -uni
σ	0.76	0.78	0.82	0.85	0.88	0.82	0.84	0.77
f_t	1	1.51	2.34	2.66	2.93	2.33	2.30	1.74
$T_{tsr,s}$/°C	21.66	18.56	20.49	22.15	23.20	20.73	21.41	18.17
$T_{tsr,r}$/°C	–	18.9	20.22	21.25	22.01	20.19	20.87	18.97

$T_{tsr,s}$ and $T_{tsr,r}$ are the relative stable temperatures during HS and HR.

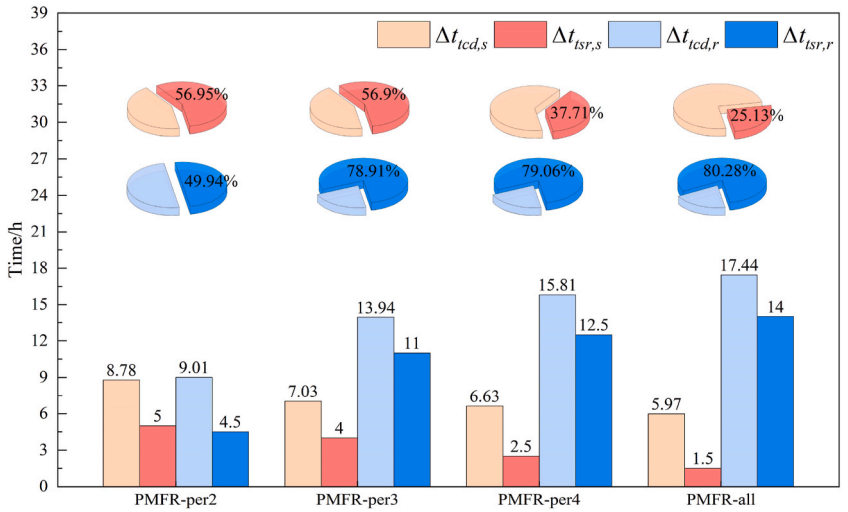

Fig. 7. Duration time of room thermal comfort and temperature stable range for different heating powers.

power, the room retains heat for longer. The prolonged heating of the perimeter of the floor results in a more pronounced overheating problem. The maximum $T_{f,sur}$ value rises, accompanied by an increase in temperature differential. When the heating power is only 28.4 %, the maximum $T_{f,sur}$ value is about 49 °C, and the maximum temperature difference reaches 27.4 °C. When the heating power increases to 86.4 %, the maximum $T_{f,sur}$ value drops to 35 °C, and the maximum temperature difference is reduced by about 13 °C. However, for the fully heated PMFR-all, the difference between the $T_{f,sur}$ values does not exceed 6 °C.

Based on the above floor surface temperature distribution law, the study selected the center point of the floor, noted as 'floor6' (x = 2400 mm, y = 1650 mm), and five measurement points 'floor1~5' at equal spacing intervals, as shown in Fig. 9. For comparative analysis, the dimensionless time t^*, which is the ratio of any moment to the total HST and HRT, is used [45]. Fig. 10 shows the variation of $T_{f,sur}$ at various points with time for different heating powers. Throughout the entire process of HS and HR, a considerable discrepancy exists in temperature between the various points on the floor with local heating. The $T_{f,sur}$ value directly above the heated zone is always larger than that of the non-heated zone. The temperature of the non-heated zone remains essentially unchanged. The temperature difference between the points is mainly generated by the temperature change of the heated area on the floor surface. The temperature difference gradually increases as the HS proceeds and reaches a maximum after the heating is stopped, and then the

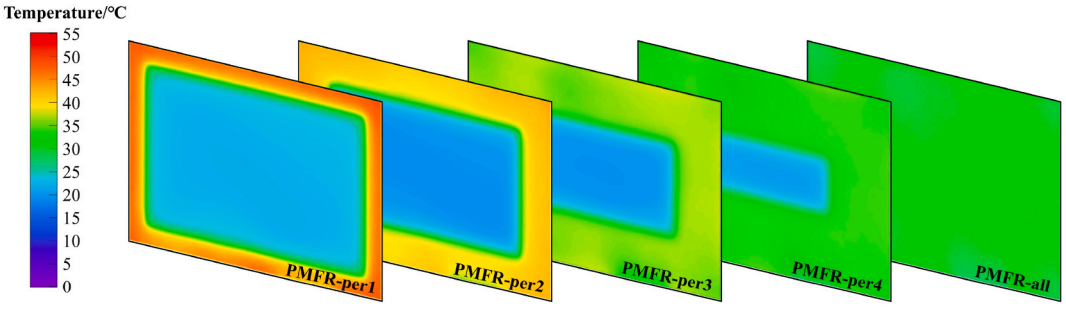

Fig. 8. Temperature distribution of floor surface at the end of HS for different heating powers.

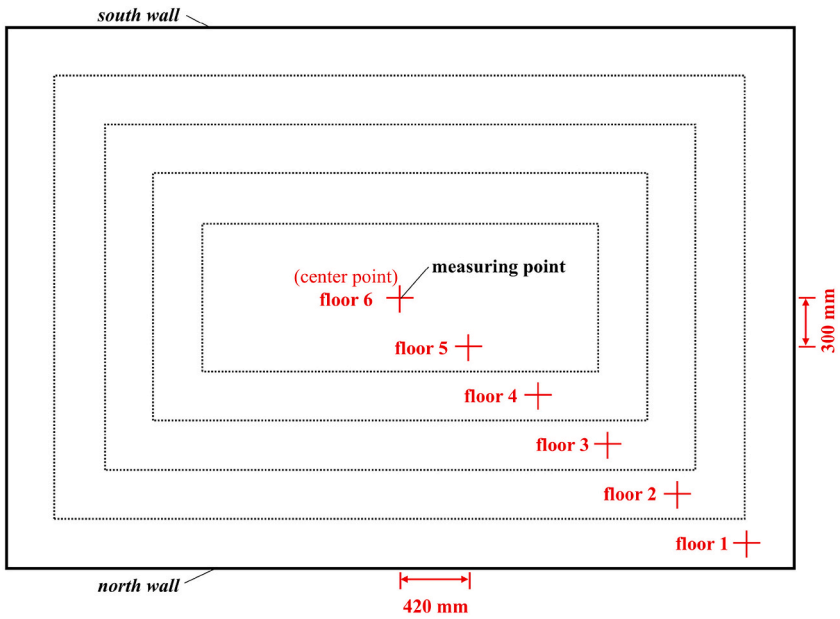

Fig. 9. Distribution of measurement points on floor surface.

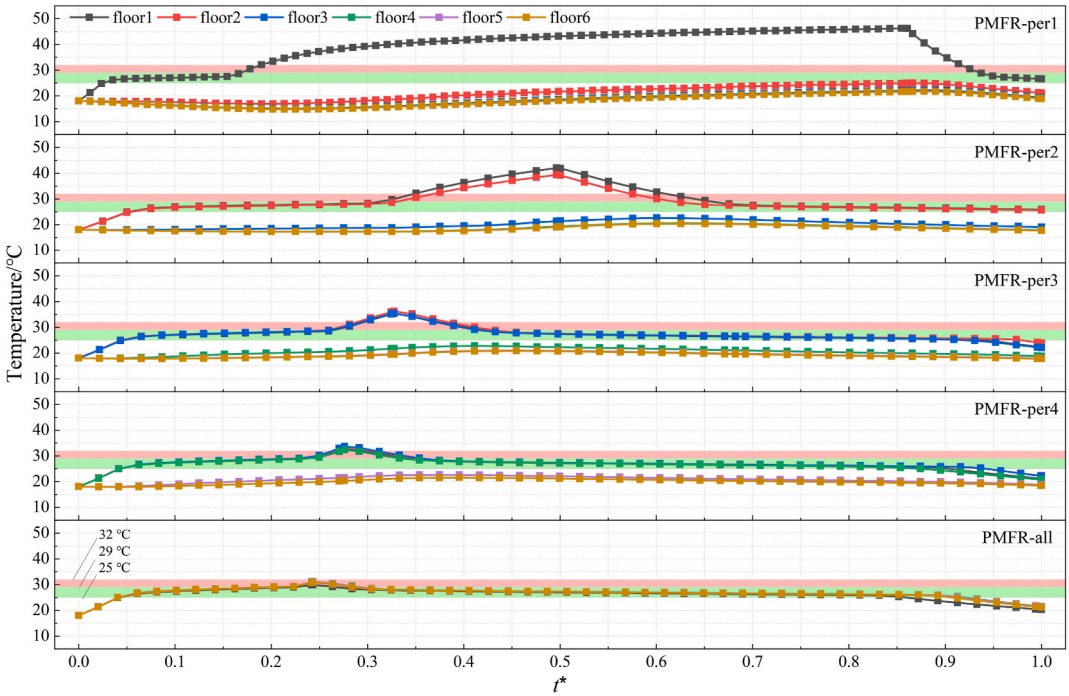

Fig. 10. Variation of floor surface temperature with time for different heating powers.

temperature difference declines until the end of the HR. The temperature difference is also stabilized for a period during the HS and HR process due to the thermal inertia of PCM during this period. In addition, the $T_{f,sur}$ value should normally not be less than 25 °C, and the upper limit of $T_{f,sur}$ should not exceed 29 °C and 32 °C for frequent and short-term stays of personnel [46]. As illustrated in the figure, the floor surface of PMFR-all can satisfy this temperature requirement better. For the other rooms (PMFR-per1∼4), the $T_{f,sur}$ in the non-heated zones fails to reach the lower temperature limit. Additionally, as the heating power decreases, the $T_{f,sur}$ in the heated zone gradually exceeds the upper temperature limit. When the heating power is greater than 71.6 %, the heated zone's $T_{f,sur}$ can be basically maintained at 25–32 °C. However, when the heating power is less than 52.3 %, the heated zone's $T_{f,sur}$ will remain above 32 °C for a

long time.

3.1.2. Energy efficiency analysis

Due to the large size difference of the PCM layer, with a length and width of 4800 mm × 3300 mm and a thickness of only 20 mm, the phase change variation of the PCM along the vertical direction is relatively minimal. Therefore, the study only analyzes the melting of PCM in the horizontal direction. Fig. 11 shows the PCM liquid fraction in the middle plane of the PCM layer at the end of the HS. It can be clearly seen that the PCM located above the heating position melts better and is able to melt completely. The phase change of the PCM at the center is poor and essentially does not occur. The lower the heating power, the smaller the heated zone, and the worse the overall melting effect of PCM. When heated at full power (PMFR-all), the PCM liquid fraction can reach 1, i.e., all PCM is completely melted. However, when the heating power is only 28.4 %, the liquid fraction of PCM is only 0.32. In addition, the thermostatic properties of PCM during melting and solidification lead to the creation of a room temperature stable range. Therefore, the better the melting situation, the more the amount of PCM maintained at PCT (28–30 °C), and the PCM's average temperature is relatively higher, which leads to the consequent increase in the T_{tsr} value described above.

The melting degree of PCM is directly related to the LHS of the PCF. As shown in Fig. 12, the thermal storage of the PCF is dominated by the LHS, and the proportion of the LHS to the THS at different heating powers is more than 60 %. In PMFR-per3, the share of LHS can reach up to 74.63 %. Since the melting effect of the PCM improves with increasing heating power (Fig. 11), the LHS capacity of the PCM increases, which consequently results in an augmented THS capacity of the PCF. The increased LHS is the main reason for the rise of the THS. The SHS capacity not only occupies a small proportion of the THS capacity but also changes relatively little under different heating powers. Unlike the change in LHS of almost 30 kJ, the change in SHS in the room is only about 2 kJ. Therefore, the impact of changes in SHS on the THS capacity is relatively minimal. In addition, the more heat the PCF stores during HS, the more heat it can utilize during HR. The more complete the melting of PCM is, the longer the solidification process takes. Therefore, higher heat storage capacity and better PCM melting situation at high heating power are also the main reasons for the increased HRT and larger Δt_{tcd} and Δt_{tsr} values in the above rooms.

Fig. 13 shows the variation of average daily electricity consumption, energy saving rate, and average daily electricity cost of the room with heating power. Although the PMFR-per1 & 2 have less heating power, their longer HST and too short HRT result in a higher $Q_{E,d}$ value of up to about 21.7 kWh/day. However, higher heating power is not always better. The PMFR-per 3 & 4 have less heating power and less variation in HST compared to PMFR-all. As a result, both of them have reduced $Q_{E,d}$ values, with a minimum of only 19.71 kWh/day, which is 0.55 kWh/day less than PMFR-all. Using PMFR-all as reference room2, the E values of the room are analyzed for different heating powers. From Fig. 13, there is an optimum value for the room's energy saving rate. In this study, the best energy saving in the room is achieved when the heating power is 71.6 %, and its energy saving compared to full heating (PMFR-all) is about 2.7 %. However, when the heating power is too low (<52.3 %), the energy efficiency of the room becomes quite poor. In addition, peak and valley electricity are used for heating according to the relevant electricity price policy. The price of electricity is 0.52 ¥/kWh for the peak period from 7:00 to 21:00 and 0.40 ¥/kWh for the valley period from 21:00 to 7:00 [47]. Since valley electricity is frequently utilized for HS in PCFRs, the electric heating film is turned on during the valley period in all rooms. The rooms' C_d values are shown in Fig. 13. Among them, the HST of PMFR-per2~4 and PMFR-all is less than 10 h, and the electric heating films are operated during the valley electricity period. However, the HST of PMFR-per1 reaches 36.18 h, causing the electric heating film to operate part of the time during the peak electricity period, which leads to its higher operating costs. The C_d value of the room does not decrease consistently with decreasing heating power. The too-low heating power allows the electric heating film to run for a longer time and shut down for a shorter time, and the C_d value rises instead, e.g., PMFR-per2. In this study, when the heating power is 71.6 %, the C_d value is minimized to about 7.88 ¥/day.

3.2. Influence of different heating positions and different surface materials

The above analysis shows that different heating powers (28.4 %–100 %) have an impact on indoor thermal comfort and energy efficiency. In this study, when the heating power is 71.6 %, the PCFR has better heating performance. Therefore, this heating power was used in the study for all subsequent comparative analyses of heating positions and surface materials.

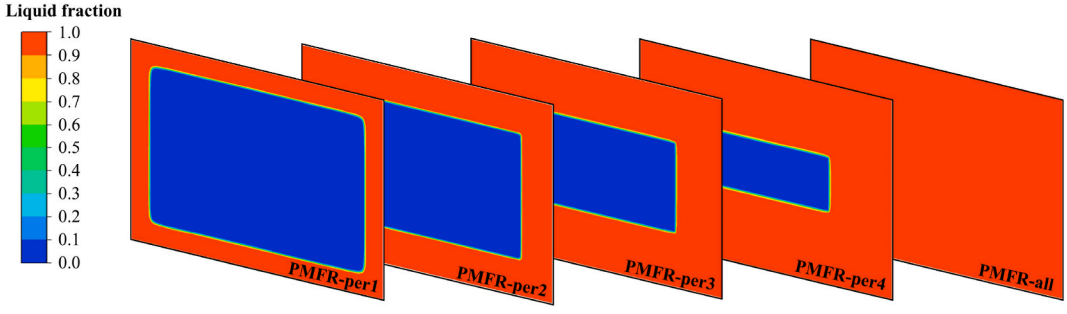

Fig. 11. Liquid fraction of PCMs at the end of HS for different heating powers.

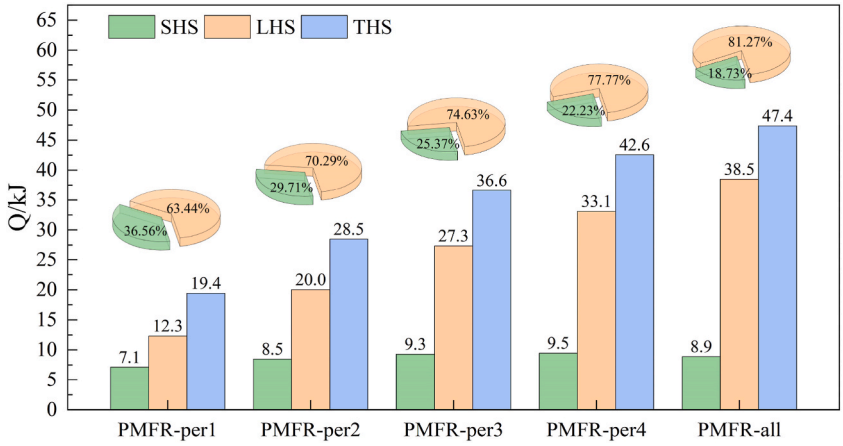

Fig. 12. Heat storage capacity of PCM for different heating powers.

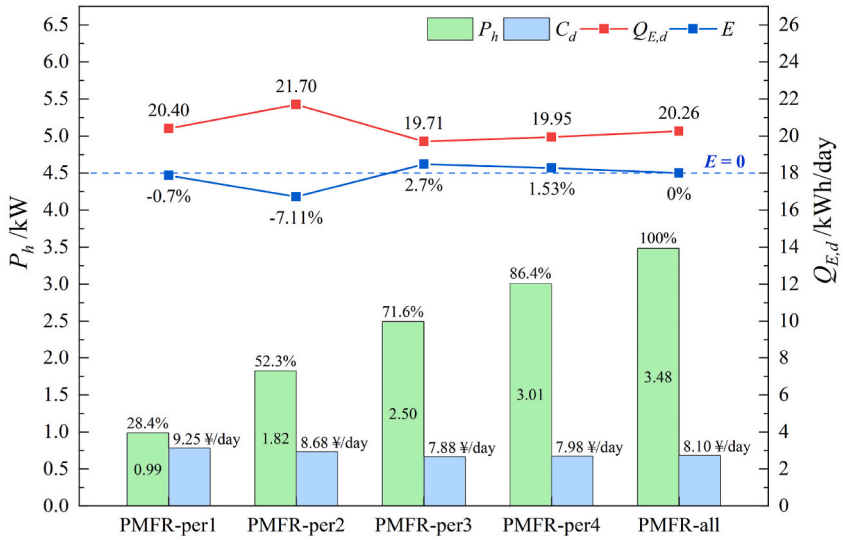

Fig. 13. Average daily electricity consumption, energy saving rate and average daily electricity cost of rooms for different heating powers.

3.2.1. *Thermal comfort analysis*

As illustrated in Fig. 14, when the heating position of the PCF is changed, although the average indoor temperature trend over time of PMFR-cen and PMFR-uni is basically the same as that of PMFR-per3, the HST and HRT of both are relatively shortened. The HST for both PMFR-cen and PMFR-uni is about 7.47 h, while the HRT is 15.28 h and 14.98 h, respectively. Moreover, the average indoor temperature of PMFR-uni is generally greater than that of PMFR-per3 and PMFR-cen during the HS and HR processes. Due to the lower thermal conductivity of wood and the effect of the room being subjected to low outdoor temperatures, the PWFR-uni stays at a lower average indoor temperature (<18 °C) for a longer period while storing heat. The temperature will continue to rise for a longer period, up to 25 °C or more, after the heating is stopped. Compared to PMFR-uni, PWFR-uni has a longer HST and a shorter HRT of 7.9 h and 12.1 h, respectively.

PMFR-per1 is used as reference room1. From Table 3 and Fig. 15, when the heating position is varied, the σ and f_t values of the room basically do not change with it, remaining around 0.83 and 2.32, respectively. However, the T_{tsr} value of PMFR-uni is about 0.5 °C higher than that of PMFR-per3 and PMFR-cen. Moreover, the thermal comfort duration time of PMFR-per3, PMFR-cen and PMFR-uni during HS and HR are roughly equal, with thermal comfort duration time being about 7.2 h for HS and about 13.8 h for HR. Nevertheless, their Δt_{tsr} values differ, as shown in Fig. 15. The Δt_{tsr} values of PMFR-per3, PMFR-cen, and PMFR-uni are gradually reduced, and correspondingly the share of thermal comfort duration time is also decreasing. In addition, for PWFR-uni, its σ and f_t values are both low at 0.77 and 1.74, respectively, due to its average indoor temperatures below 18 °C and above 24 °C over an extended period and the shorter HRT (Fig. 14). During the HS process, although the average indoor temperature of PWFR-uni experiences a period of stable temperature, the temperature does not reach 18 °C for a long time, so the $T_{tsr,s}$ value is extremely low, and the $\Delta t_{tcd,s}$ and $\Delta t_{tsr,s}$ values are also extremely small. During HR, the $T_{tsr,r}$ of PWFR-uni is reduced by about 1.9 °C compared with that of

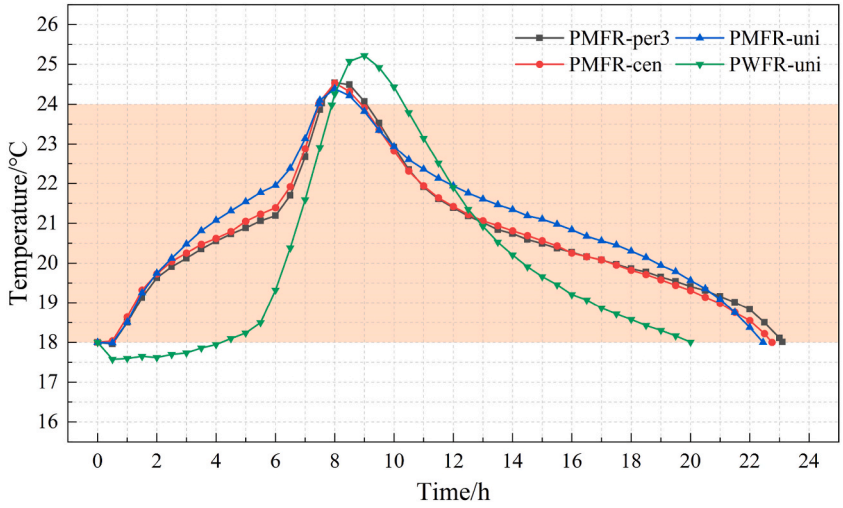

Fig. 14. Variation of average indoor temperature with time for different heating positions and surfacing materials.

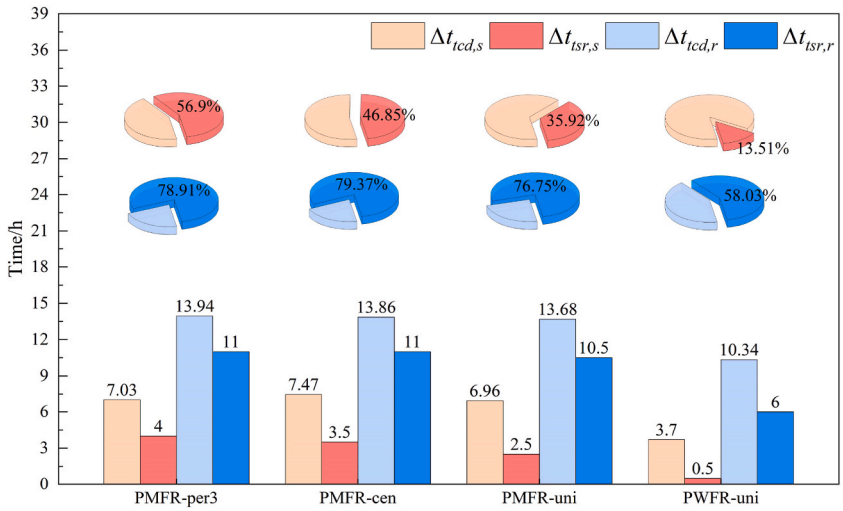

Fig. 15. Duration time of indoor thermal comfort and temperature stable range for different heating positions and surface materials.

PMFR-uni, and the $\Delta t_{tcd,r}$ and $\Delta t_{tsr,r}$ values are reduced by about 3.3–4.5 h.

The distribution of $T_{f,sur}$ at different heating positions and surface materials is shown in Fig. 16. While the $T_{f,sur}$ values of PMFR-per3, PMFR-cen, PMFR-uni, and PWFR-uni all follow the regular pattern of higher temperatures at the heated zones and lower temperatures at the non-heated zones, the $T_{f,sur}$ values of these four rooms differ in magnitude. The maximum $T_{f,sur}$ value of PMFR-cen

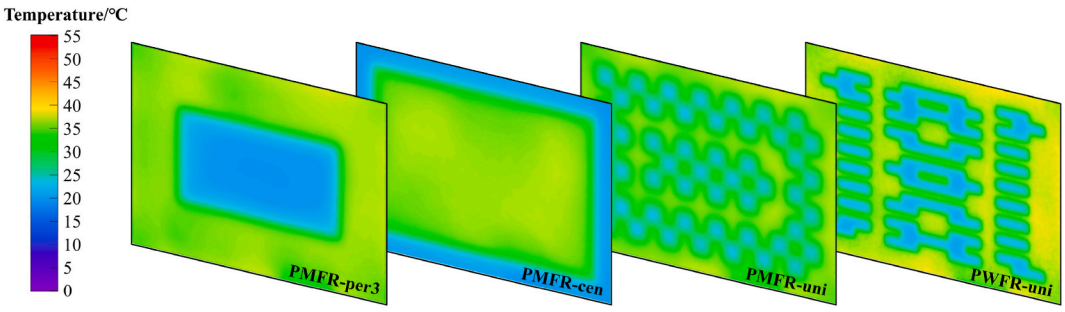

Fig. 16. Temperature distribution of floor surface at the end of HS for different heating positions and surface materials.

is about 37.08 °C, which is slightly lower than that of PMFR-per3, but the minimum $T_{f,sur}$ values of both are essentially the same. However, PMFR-uni achieves a minimum $T_{f,sur}$ value of 23.58 °C, which is about 4 °C higher than PMFR-per3 and PMFR-cen, and their maximum temperature is essentially the same, i.e., the temperature difference between the floor surfaces is reduced. In addition, for the PWFR-uni that also uses uniform heating, while the minimum $T_{f,sur}$ value rises, the maximum temperature also becomes higher, exceeding 39 °C. Therefore, its floor surface temperature difference remains high at about 18.8 °C.

Fig. 17 represents the variation of $T_{f,sur}$ with time. In conjunction with Fig. 10, varying the heating position influences the change in $T_{f,sur}$ during the HS and HR processes. The $T_{f,sur}$ values above the heated zone in PMFR-per3 and PMFR-cen are maintained at 25–32 °C for a long time, but the $T_{f,sur}$ values above the non-heated zone are very low, about 20 °C. However, in PMFR-uni, the temperature difference between points on the floor surface is reduced, while the point temperature on the floor surface above the non-heated zone increases. This enables the required thermal comfort temperature to be reached within a certain period. In addition, different surface materials can affect the change of the $T_{f,sur}$ value during HS and HR. Compared to the PMFR-uni, the PWFR-uni's $T_{f,sur}$ values at various points are less likely to reach thermal comfort temperatures, with $T_{f,sur}$ failing to reach 25 °C for longer periods, both above the heated and non-heated zones.

3.2.2. Energy efficiency analysis

As shown in Fig. 18, the PCM melting situation strongly depends on the heating position of the floor. The PCM located above the heated zone melts more completely. Due to PCM's low thermal conductivity and poor horizontal heat transfer, the PCM above the non-heated zone fails to completely undergo phase change by the end of the HS. The liquid fraction of PMFR-per3, PMFR-cen and PMFR-uni at the end of the HS is about 0.7, which is less than their heating power percentage of 71.6 %. This indicates that the PCM above their non-heated zone is basically not melted. The PCM melting situation of PWFR-uni is slightly better than that of the other three, with a liquid fraction of about 0.73. In addition, Fig. 19 demonstrates the variation of PCM liquid fraction with time for different surface materials. As shown in the figure, the PCM within the PWFR-uni melts faster and more completely than the PCM in the PMFR-uni. This is because the thermal conductivity of wood floor is lower than that of marble floor. Although their heating power is the same, the heat transferred through the wood floor to the room at the same time is less than through the marble floor. Therefore, more heat is absorbed by PCM under the wood floor. This is also the reason why the PWFR-uni's $T_{f,sur}$ values mentioned above are relatively lower (Fig. 17) and why the average indoor temperatures struggle to reach 18 °C for long period of time (Fig. 14). When releasing heat, similarly due to the low thermal conductivity of wood floor, although the PCM stores a large amount of latent heat, it is difficult to release it to the room through the wood floor. Therefore, this causes both a slower solidification of the PCM and a rapid decrease in average indoor temperature within the PWFR-uni. At the completion of the HR, the PCM liquid fraction within the PWFR-uni is about 0.28, indicating

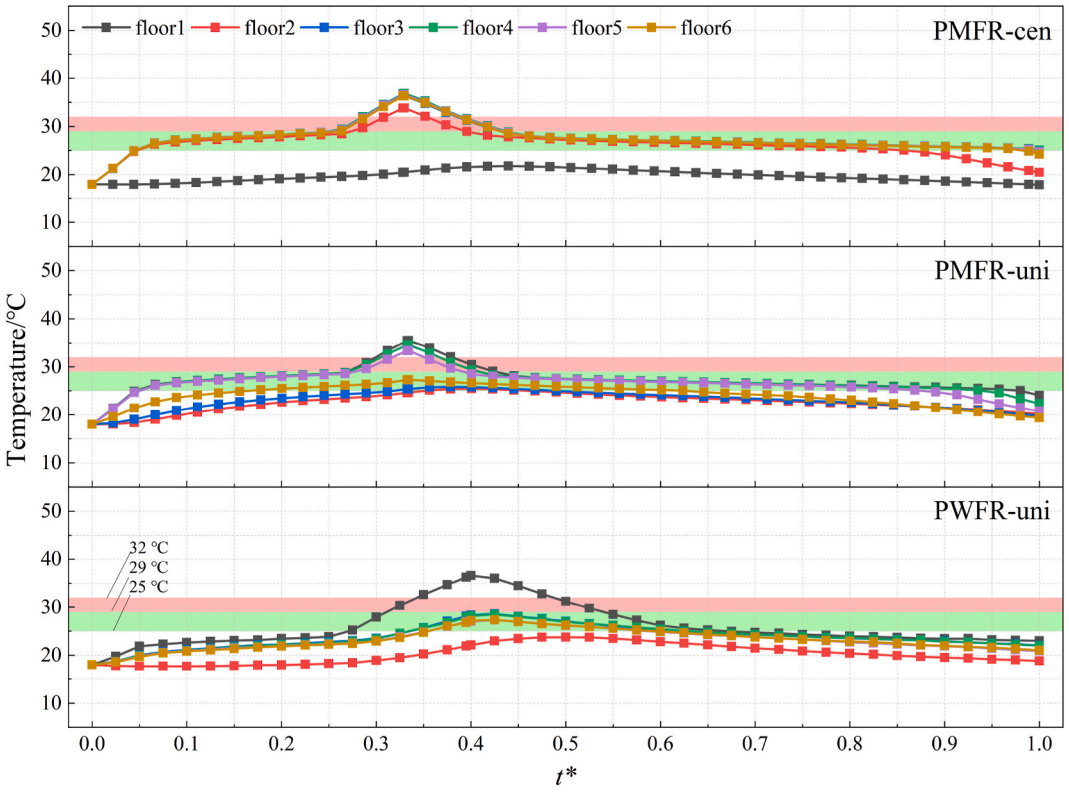

Fig. 17. Variation of floor surface temperature with time for different heating positions and surface materials.

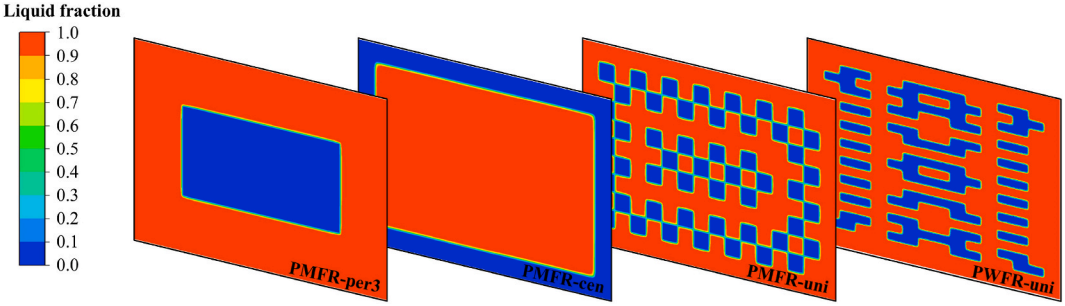

Fig. 18. Liquid fraction of PCMs at the end of HS for different heating positions and surface materials.

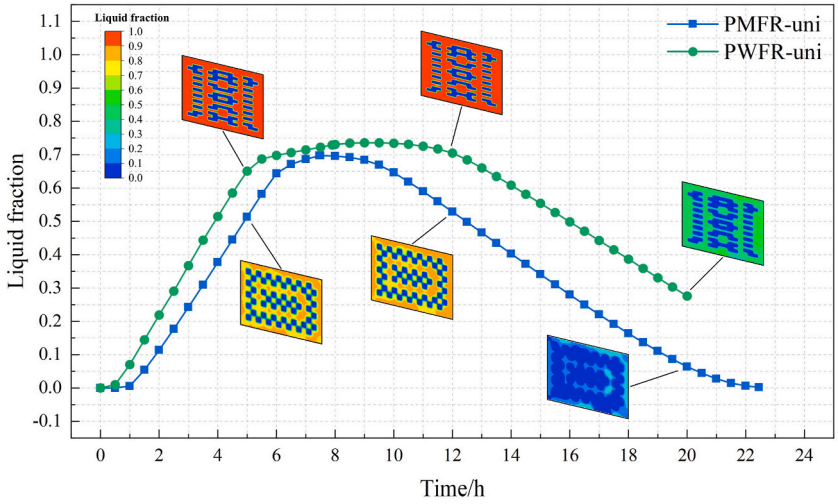

Fig. 19. Variation of PCM liquid fraction with time for different surface materials.

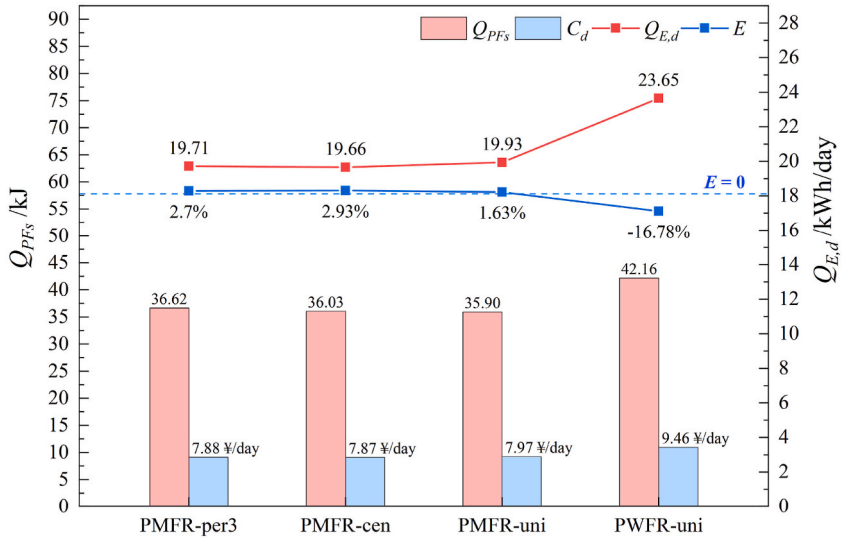

Fig. 20. Heat storage capacity, average daily electricity consumption, energy saving rate and average daily electricity cost of rooms for different heating positions and surface materials.

that its stored latent heat is not fully released.

As shown in Fig. 20, the impact of heating position variation on the HS capacity of the PCF is relatively weak. Since the PCM liquid fraction at the completion of HS is essentially the same for PMFR-per3, PMFR-cen, and PMFR-uni, the heat storage capacities of the three are also approximately equal, with a difference of no more than 0.8 kJ. The heat storage capacity of PWFR-uni is improved, being about 6.26 kJ higher than that of PMFR-uni. However, after the above analysis, the liquid fraction of PWFR-uni at the end of HS increases by only 0.03. The increase in heat storage capacity of PWFR-uni is not primarily dependent on the improved melting effect of the PCM but stems more from the increased temperature of the fully melted PCM above the heated zone. Among the increased heat storage capacity, the SHS capacity increases by about 5.1 kJ and the LHS capacity increases by only about 1.2 kJ. In addition, the $Q_{E,d}$, E, and C_d values for the three rooms with different heating positions are also less variable, with maximum increases of no more than 0.3 kWh/day, 1.3 %, and 0.1 ¥/day, respectively. PMFR-uni has the largest $Q_{E,d}$ and C_d, but they do not exceed 20 kWh/day and 8 ¥/day, respectively. It also achieves an E value of 1.63 % compared to reference room2 (PMFR-all). Meanwhile, the PWFR-uni's electric heating film operates for a longer period, and it can maintain a shorter HRT. Therefore, its average daily electricity consumption is higher. The PWFR-uni is not energy efficient compared to reference room2 and has higher average daily electricity cost.

4. Conclusions

The study designed different local heating methods based on the ability of PCF modules to supply heat flexibly and proposed evaluation indicators to quantitatively analyze the room temperature stable range of PCFRs in terms of both temperature and time. The study simulated and analyzed eight types of electrically heated PCF heating rooms. The effects of different heating powers, heating positions, and surface materials on the thermal comfort and energy efficiency of the room under local heating methods were investigated. Investigating and determining the suitable local heating method can provide a reference for the actual engineering design, further reduce the energy consumption and operational cost of PCF heating, and promote the wide application of PCFs in buildings. The following conclusions are summarized.

(1) Variations in heating power can have a large impact on the thermal comfort of the PCFR. As heating power increases, the HST of the PCF shortens, and the HRT increases. The σ, f_t, T_{tsr} and Δt_{tsr} values all rise accordingly. There is an optimum value for heating power. The energy efficiency of the room does not continue to improve with increasing heating power. In this study, the appropriate heating power selected under the local heating method is 71.6 %. The average daily electricity consumption under this heating power is the lowest at 19.71 kWh/day. Average daily electricity cost is also the lowest at 7.88 ¥/day.
(2) The variation of the heating position mainly influences the thermal comfort of the PCFRs, whereas the impact on energy efficiency is relatively weak. Compared with PMFR-per3 and PMFR-cen, PMFR-uni has a more favorable heating position arrangement. Its T_{tsr} value increases by about 1 °C. Moreover, the floor surface temperature above the non-heated zone increases by about 4 °C, and the temperature difference on the floor surface is reduced. The duration time for which the floor surface thermal comfort temperature requirement can be met is also prolonged to a certain extent. In addition, the average daily electricity consumption, energy savings, and average daily electricity costs of the three PMFRs are essentially equal.
(3) The thermal comfort and energy efficiency of the PMFR are superior to those of the PWFR. Compared with PMFR-uni, PWFR-uni has longer HST and shorter HRT. Its average indoor temperature is lower, failing to reach 18 °C for a long time. The σ, f_t, T_{tsr} and Δt_{tsr} values of PMFR-uni are also smaller. Moreover, the temperature difference on the floor surface remains large, about 18.8 °C. Compared with PMFR-all, PWFR-uni fails to realize the energy saving purpose, and its average daily electricity consumption and cost are higher, exceeding 23 kWh/day and 9 ¥/day, respectively.

CRediT authorship contribution statement

Tianyu Wang: Writing – review & editing, Writing – original draft, Visualization, Resources, Methodology, Investigation, Formal analysis, Data curation, Conceptualization. **Haichao Wang:** Writing – review & editing, Supervision, Resources, Project administration, Funding acquisition. **Zhiwen Luo:** Writing – review & editing, Resources, Conceptualization.

Declaration of competing interest

The authors declare that they have no known competing financial interests or personal relationships that could have appeared to influence the work reported in this paper.

Acknowledgements

This work was supported by the China National Key Research and Development Program – China-Finland intergovernmental cooperation in science and technology innovation (2021YFE0116200), academy research fellow funding from Research Council of Finland (Funding No. 334205 and 358055) and NSFC-RS international exchange projects: Digital-twin based smart control of low-carbon heating under climate change (NSFC funding NO. 52311530087 and RS funding NO. 223541).

Data availability

No data was used for the research described in the article.

References

[1] Energy Institute, Statistical review of world energy. https://www.energyinst.org/statistical-review, 2023. (Accessed 10 October 2024), 2023.
[2] International Energy Agency, CO_2 emissions in 2023. https://www.iea.org/reports/co2-emissions-in-2023, 2023. (Accessed 10 October 2024).
[3] X. Qian, R. Lu, Domestic and International Oil and Gas Industry Development Report 2023, Petroleum industry press, 2023. http://etri.cnpc.com.cn/etri/gzdt/news.shtml. (Accessed 10 October 2024).
[4] International Energy Agency, Tracking clean energy progress. https://www.iea.org/reports/tracking-clean-energy-progress-2023, 2023. (Accessed 10 October 2024), 2023.
[5] A.G. Anter, A.A. Sultan, A.A. Hegazi, M.A. El Bouz, Thermal performance and energy saving using phase change materials (PCM) integrated in building walls, J. Energy Storage 67 (2023) 107568, https://doi.org/10.1016/j.est.2023.107568.
[6] W. Chen, Y. Liu, X. Liang, F. Luo, T. Liao, S. Wang, X. Gao, Z. Zhang, Y. Fang, Experimental and numerical investigations on radiant floor heating system integrated with macro-encapsulated phase change material, Energy 282 (2023) 128375, https://doi.org/10.1016/j.energy.2023.128375.
[7] M. Barrio, J. Font, D.O. Lhpez, J. Muntasell, J. Ll Tamarit, Floor radiant system with heat storage by a solid-solid phase transition material, Sol. Energy Mater. Sol. Cells 27 (1992) 127–133, https://doi.org/10.1016/0927-0248(92)90115-6.
[8] X. Sui, H. Liu, Z. Du, S. Yu, Developing a TRNSYS model for radiant cooling floor with a pipe-embedded PCM layer and parametric study on system thermal performance, J. Energy Storage 71 (2023) 108024, https://doi.org/10.1016/j.est.2023.108024.
[9] H. Salt, Preliminary design considerations for a rockbed/floor space-heating system, Build. Environ. 20 (1985) 221–231, https://doi.org/10.1016/0360-1323(85)90037-X.
[10] B. Sun, Y. Xu, Y. Zhang, H. Zhao, X. Liu, Simulation and optimization research of double energy storage floor based on heat transfer characteristic of phase change materials, J. Energy Storage 51 (2022) 104452, https://doi.org/10.1016/j.est.2022.104452.
[11] K. Lin, Y. Zhang, X. Xu, H. Di, R. Yang, P. Qin, Modeling and simulation of under-floor electric heating system with shape-stabilized PCM plates, Build. Environ. 39 (2004) 1427–1434, https://doi.org/10.1016/j.buildenv.2004.04.005.
[12] X. Jin, X. Zhang, Thermal analysis of a double layer phase change material floor, Appl. Therm. Eng. 31 (2011) 1576–1581, https://doi.org/10.1016/j.applthermaleng.2011.01.023.
[13] Y. Zhou, S. Zheng, H. Chen, G. Zhang, Thermal performance and optimized thickness of active shape-stabilized PCM boards for side-wall cooling and under-floor heating system, Indoor Built Environ. 25 (2016) 1279–1295, https://doi.org/10.1177/1420326X16671983.
[14] M. Zhao, T. Zhu, C. Wang, H. Chen, Y. Zhang, Numerical simulation on the thermal performance of hydraulic floor heating system with phase change materials, Appl. Therm. Eng. 93 (2016) 900–907, https://doi.org/10.1016/j.applthermaleng.2015.10.020.
[15] Q. Zhang, Z. Yang, G. Wang, Numerical and experimental investigation on dynamic thermal performance of floor heating system with phase change material for thermal storage, Indoor Built Environ. 30 (2021) 621–634, https://doi.org/10.1177/1420326X19900535.
[16] X. Jin, X. Zhang, Thermal analysis of a double layer phase change material floor, Appl. Therm. Eng. 31 (2011) 1576–1581, https://doi.org/10.1016/j.applthermaleng.2011.01.023.
[17] X. Xu, Y. Zhang, K. Lin, H. Di, R. Yang, Modeling and simulation on the thermal performance of shape-stabilized phase change material floor used in passive solar buildings, Energ. Buildings 37 (2005) 1084–1091, https://doi.org/10.1016/j.enbuild.2004.12.016.
[18] W. Fu, W. Zhou, G. Lv, R. Zhang, H. Peng, T. Fang, J. Liu, W. Chen, Y. Fang, Phase change temperature adjustment of $CH_3COONa{\cdot}3H_2O$ to fabricate composite phase change material for radiant floor heating, Case Stud. Therm. Eng. 42 (2023) 102773, https://doi.org/10.1016/j.csite.2023.102773.
[19] B. Wang, W. Zhou, J. Wu, L. Sun, M. Wang, W. Zhang, A phase change thermal storage material and its performance for floor electric heating system, J. Energy Storage 59 (2023) 106518, https://doi.org/10.1016/j.est.2022.106518.
[20] K. Faraj, M. Khaled, J. Faraj, F. Hachem, K. Chahine, C. Castelain, Energetic and economic analyses of integrating enhanced macro-encapsulated PCM's with active underfloor hydronic heating, Energy Rep. 8 (2022) 848–862, https://doi.org/10.1016/j.egyr.2022.07.099.
[21] R. Ansuini, R. Larghetti, A. Giretti, M. Lemma, Radiant floors integrated with PCM for indoor temperature control, Energ. Buildings 43 (2011) 3019–3026, https://doi.org/10.1016/j.enbuild.2011.07.018.
[22] W. Sun, Y. Zhang, Z. Ling, X. Fang, Z. Zhang, Experimental investigation on the thermal performance of double-layer PCM radiant floor system containing two types of inorganic composite PCMs, Energ. Buildings 211 (2020) 109806, https://doi.org/10.1016/j.enbuild.2020.109806.
[23] G. Zhou, J. He, Thermal performance of a radiant floor heating system with different heat storage materials and heating pipes, Appl. Energy 138 (2015) 648–660, https://doi.org/10.1016/j.apenergy.2014.10.058.
[24] H. Kitagawa, T. Asawa, M.A.D. Rio, T. Kubota, A.R. Trihamdani, Thermal energy simulation of PCM-based radiant floor cooling systems for naturally ventilated buildings in a hot and humid climate, Build. Environ. 238 (2023) 110351, https://doi.org/10.1016/j.buildenv.2023.110351.
[25] Z. Liu, Z. Wei, R. Teng, H. Sun, Z. Qie, Research on performance of radiant floor heating system based on heat storage, Appl. Therm. Eng. 231 (2023) 120812, https://doi.org/10.1016/j.applthermaleng.2023.120812.
[26] S. Baek, S. Kim, Determination of optimum hot-water temperatures for PCM radiant floor-heating systems based on the wet construction method, Sustainability 10 (2018) 4004, https://doi.org/10.3390/su10114004.
[27] W. Heng, Z. Wang, Y. Wu, Experimental study on phase change heat storage floor coupled with air source heat pump heating system in a classroom, Energ. Buildings 251 (2021) 111352, https://doi.org/10.1016/j.enbuild.2021.111352.
[28] K. Faraj, M. Khaled, J. Faraj, F. Hachem, C. Castelain, Experimental study on the use of enhanced coconut oil and paraffin wax phase change material in active heating using advanced modular prototype, J. Energy Storage 41 (2021) 102815, https://doi.org/10.1016/j.est.2021.102815.
[29] J. Li, P. Xue, H. He, W. Ding, J. Han, Preparation and application effects of a novel form-stable phase change material as the thermal storage layer of an electric floor heating system, Energ. Buildings 41 (2009) 871–880, https://doi.org/10.1016/j.enbuild.2009.03.009.
[30] R. Barzin, J.J.J. Chen, B.R. Young, M.M. Farid, Application of PCM underfloor heating in combination with PCM wallboards for space heating using price based control system, Appl. Energy 148 (2015) 39–48, https://doi.org/10.1016/j.apenergy.2015.03.027.
[31] S. Cesari, G. Emmi, M. Bottarelli, A weather forecast-based control for the improvement of PCM enhanced radiant floors, Appl. Therm. Eng. 206 (2022) 118119, https://doi.org/10.1016/j.applthermaleng.2022.118119.
[32] X. Kong, L. Jiang, L. Guo, N. Wang, J. Ren, Experimental study on the performance of a stepped phase-change radiation terminal integrated with a building used in summer and winter, J. Energy Storage 62 (2023) 106860, https://doi.org/10.1016/j.est.2023.106860.
[33] Y. Qu, D. Zhou, F. Xue, L. Cui, Multi-factor analysis on thermal comfort and energy saving potential for PCM-integrated buildings in summer, Energ. Buildings 241 (2021) 110966, https://doi.org/10.1016/j.enbuild.2021.110966.
[34] T. Wang, H. Wang, A. Wang, R. Lahdelma, G. Wang, J. Han, A comprehensive review on building integrated phase change floors with phase change materials for energy storage and indoor environment control, J. Energy Storage 98 (2024) 112928, https://doi.org/10.1016/j.est.2024.112928.
[35] H. Wang, S. Bo, C. Zhu, P. Hua, Z. Xie, C. Xu, T. Wang, X. Li, H. Wang, R. Lahdelma, K. Granlund, E. Teppo, A zoned group control of indoor temperature based on MPC for a space heating building, Energ. Conver. Manage. 290 (2023) 117196, https://doi.org/10.1016/j.enconman.2023.117196.
[36] China Academy of Building Science, Code for Thermal Design of Civil Buildings (GB50176-2016), 2016.
[37] O. Babaharra, K. Choukairy, S. Hamdaoui, K. Khallaki, S.H. Mounir, Thermal behavior evaluation of a radiant floor heating system incorporates a microencapsulated phase change material, Construct, Build Mater 330 (2022) 127293, https://doi.org/10.1016/j.conbuildmat.2022.127293.
[38] Dongguan Chengbang Polymer Material Co. Guangdong, China. https://rl9ym1en.51pla.com/product.htm, (accessed 10 October 2024).

[39] Shandong Weimengshi Technology Co, Temperature and humidity transmitter (Probe 485 type), China. https://www.sdvms.com/index.php?a=shows&catid=76&id=17. (Accessed 26 January 2025).
[40] J. Guo, Y. Jiang, A semi-analytical model for evaluating the thermal storage capacity and heat use efficiency of flexible thermal storage heating floor, Appl. Therm. Eng. 198 (2021) 117448, https://doi.org/10.1016/j.applthermaleng.2021.117448.
[41] Y. Liu, Z. Tian, C. Song, Y. Chen, Y. Li, J. Liu, Thermal performance and optimization of a casing pipe solar energy storage floor with phase change material, Energ. Buildings 247 (2021) 111167, https://doi.org/10.1016/j.enbuild.2021.111167.
[42] T. Xu, J. Zhang, G. Fan, T. Zou, H. Hu, Y. Du, Y. Yang, H. Li, P. Huang, Hydrate salt/fumed silica shape-stabilized composite phase change material with adjustable phase change temperature for radiant floor heating system, J. Build. Eng. 71 (2023) 106400, https://doi.org/10.1016/j.jobe.2023.106400.
[43] C.S. (GB), Design Code for Heating Ventilation and Air Conditioning of Civil Buildings (In Chinese), Chinese Standards (GB), 2012.
[44] L. Karim, F. Barbeon, P. Gegout, A. Bontemps, L. Royon, New phase-change material components for thermal management of the light weight envelope of buildings, Energ. Buildings 68 (2014) 703–706, https://doi.org/10.1016/j.enbuild.2013.08.056.
[45] J. Fernández-Seara, F.J. Uhıá, J. Sieres, Experimental analysis of a domestic electric hot water storage tank. Part I: static mode of operation, Appl. Therm. Eng. 27 (2007) 129–136, https://doi.org/10.1016/j.applthermaleng.2006.05.006.
[46] China Academy of Building Science, Technical Specification for Radiant Heating and Cooling (JGJ 142-2012), 2012.
[47] Dalian power supply company, electricity knowledge. https://www.dl.gov.cn/art/2023/6/20/art_222_2081646.html, 2023. (Accessed 10 October 2024).